First-principles approach to the dynamic magnetoelectric couplings for the non-reciprocal directional dichroism in BiFeO3

Jun Hee Lee, István Kézsmárki, Randy S. Fishman

PAPER • OPEN ACCESS

First-principles approach to the dynamic magnetoelectric couplings for the non-reciprocal directional dichroism in BiFeO$_3$

To cite this article: Jun Hee Lee *et al* 2016 *New J. Phys.* **18** 043025

IOP ebooks™

Bringing you innovative digital publishing with leading voices to create your essential collection of books in STEM research.

Start exploring the collection - download the first chapter of every title for free.

New Journal of Physics

CrossMark

PAPER

First-principles approach to the dynamic magnetoelectric couplings for the non-reciprocal directional dichroism in BiFeO$_3$ [*]

Jun Hee Lee[1,2], István Kézsmáki[3] and Randy S Fishman[1]

[1] Materials Science and Technology Division, Oak Ridge National Laboratory, Oak Ridge, TN 37831, USA
[2] School of Energy and Chemical Engineering, Ulsan National Institute of Science and Technology (UNIST), Ulsan 44919, Korea
[3] Department of Physics, Budapest University of Technology and Economics and MTA-BME Lendület Magneto-optical Spectroscopy Research Group, 1111 Budapest, Hungary

E-mail: **e-mail: leej@ornl.gov**

Abstract

Due to the complicated magnetic and crystallographic structures of BiFeO$_3$, its magnetoelectric (ME) couplings and microscopic model Hamiltonian remain poorly understood. By employing a first-principles approach, we uncover all possible ME couplings associated with the spin-current (SC) and exchange-striction (ES) polarizations, and construct an appropriate Hamiltonian for the long-range spin-cycloid in BiFeO$_3$. First-principles calculations are used to understand the microscopic origins of the ME couplings. We find that inversion symmetries broken by ferroelectric and antiferroelectric distortions induce the SC and the ES polarizations, which cooperatively produce the dynamic ME effects in BiFeO$_3$. A model motivated by first principles reproduces the absorption difference of counter-propagating light beams called non-reciprocal directional dichroism. The current paper focuses on the spin-driven (SD) polarizations produced by a dynamic electric field, i.e. the dynamic ME couplings. Due to the inertial properties of Fe, the dynamic SD polarizations differ significantly from the static SD polarizations. Our systematic approach can be generally applied to any multiferroic material, laying the foundation for revealing hidden ME couplings on the atomic scale and for exploiting optical ME effects in the next generation of technological devices such as optical diodes.

The exceptional characteristics exhibited by BiFeO$_3$ include its high ferroelectric ($T_C \approx 1100$ K [1]) and magnetic ($T_N \approx 640$ K [2]) transition temperatures, both well above room temperature, and its large ferroelectric (FE) polarization (~ 90 μC cm^{-2} [3]) below T_C. Below the magnetic ordering temperature T_N, antiferromagnetic order develops with a long-wavelength ($\lambda \approx 62$ nm [2]) cycloid. Surprisingly, the same characteristics that make BiFeO$_3$ so extraordinary have also hampered our understanding of the magnetoelectric (ME) effects driven by spin ordering below T_N. Despite strenuous effort [2, 4–9] and the strong ME effects recently revealed by neutron-scattering [10] and Raman-spectroscopy [11] measurements, little is known about the microscopic origins of the spin-driven (SD) polarizations and ME couplings in bulk rhombohedral BiFeO$_3$ (space group $R3c$).

Due to the lack of spatial inversion and time reversal symmetries in multiferroics, the coupling between spins and local electric dipoles creates strong ME effects [12]. Mostly studied in the static limit, ME effects are resonantly enhanced at the so-called ME spin-wave excitations or electromagnons characterized by the coupled dynamics of spins and local electric dipoles [12]. The different absorption of counter-propagating light beams called non-reciprocal directional dichroism (NDD) has proven to be a powerful tool to investigate intrinsic ME couplings in several multiferroics [13–17]. Dynamical studies are especially suited to leaky ferroelectrics where

static magneto-capacitance measurements are not feasible and to type-*I* multiferroics like $BiFeO_3$ where static magneto-capacitance measurements are often hindered by the large preexisting FE polarization.

$BiFeO_3$ has two distinctive structural distortions that remove inversion centers and couple to the electric component of light. One is the FE distortion $\Gamma_4^-[111]$ that breaks global inversion symmetry (IS). The other is the antiferroelectric (AF) octahedral rotation $R_4^+[111]$ that breaks the local IS between nearest neighbor spins. Using a first-principles approach tied to a microscopic Hamiltonian, we demonstrate that all ME couplings are microscopically driven by distinct combinations of these two inherent structural distortions.

The first-principles approach described in this paper has already laid the foundation for two previous studies of $BiFeO_3$. This approach was used [18, 19] to predict the dynamic NDD observed in $BiFeO_3$ even at room temperature. As discussed in section 3, four spin-current (SC) polarizations $\sim \mathbf{S}_i \times \mathbf{S}_j$ associated with FE and AF distortions cooperatively induce the strong NDD in $BiFeO_3$. This approach was also used [20] to predict that the static SD polarization $-3\ \mu C\ cm^{-2}$ in $BiFeO_3$ points opposite to the preexisting FE polarization. A record high among all known multiferroics, this SD polarization is produced by the ES contribution $\sim \mathbf{S}_i \cdot \mathbf{S}_j$ discussed in section 4.

1. Microscopic spin-cycloid model for BiFeO₃

The FE polarization $\mathbf{P}^{FE} \| \mathbf{z}'$ emerging below T_C can take eight different orientations along the four cubic diagonals $\mathbf{z}' = \langle 1, 1, 1 \rangle$. For a given $\mathbf{z}' = [1, 1, 1]$, the three possible orientations for the $\mathbf{x}'_m$ cycloidal modulation wavevectors are $\mathbf{x}'_1 = [1, -1, 0]$, $\mathbf{x}'_2 = [1, 0, -1]$, and $\mathbf{x}'_3 = [0, 1, -1]$ with corresponding $\mathbf{y}'_m = \mathbf{z}' \times \mathbf{x}'_m$. In magnetic domain m, the cycloidal ordering wavevectors are

$$\mathbf{Q}_m = \mathbf{Q}_0 + \frac{2\sqrt{2}\pi\delta}{a}\mathbf{x}'_m, \tag{1}$$

where $\mathbf{Q}_0 = (\pi/a)(1, 1, 1)$ is the wavevector for simple G-type antiferromagnet and $a = 3.96$ Å is the pseudo-cubic lattice constant. Hence, the ordering wavevectors are $\mathbf{Q}_1 = (2\pi/a)(0.5 + \delta, 0.5 - \delta, 0.5)$, $\mathbf{Q}_2 = (2\pi/a)(0.5 + \delta, 0.5, 0.5 - \delta)$, and $\mathbf{Q}_3 = (2\pi/a)(0.5, 0.5 + \delta, 0.5 - \delta)$. In terms of $\delta \ll 1$, the cycloidal period is $\lambda = a/(\sqrt{2}\,\delta)$.

FE and AF distortions create the DM interactions $\boldsymbol{D}_{FE}$ and $\boldsymbol{D}_{AF}$. Including all magnetic anisotropies produced by these distortions, the spin Hamiltonian can be written

$$\mathcal{H} = \mathcal{H}^{SC}_{FE} + \mathcal{H}^{SC}_{AF} + \mathcal{H}^{EX} + \mathcal{H}^{SIA}, \tag{2}$$

$$\mathcal{H}^{SC}_{FE} = \sum_{\langle i,j \rangle} \boldsymbol{D}_{FE} \cdot (\mathbf{S}_i \times \mathbf{S}_j), \tag{3}$$

$$\mathcal{H}^{SC}_{AF} = \sum_{\langle i,j \rangle} (-1)^{n_i} \boldsymbol{D}_{AF} \cdot (\mathbf{S}_i \times \mathbf{S}_j), \tag{4}$$

$$\mathcal{H}^{EX} = -J_1 \sum_{\langle i,j \rangle} \mathbf{S}_i \cdot \mathbf{S}_j - J_2 \sum_{\langle i,j \rangle'} \mathbf{S}_i \cdot \mathbf{S}_j, \tag{5}$$

$$\mathcal{H}^{SIA} = -K \sum_i (\mathbf{S}_i \cdot \mathbf{z}')^2, \tag{6}$$

where $\langle i, j \rangle$ and $\langle i, j \rangle'$ represent nearest and next-nearest neighbor spins, respectively. This is the most general Hamiltonian that includes the allowed distortions in $R3c$ $BiFeO_3$ but neglecting exchange anisotropy terms of the form

$$J_{x'}(S_{ix'}S_{jx'} + S_{iy'}S_{jy'}) + J_{z'}S_{iz'}S_{jz'},$$

which are usually small for transition metal ions with half-filled d-shell such as Fe^{3+}. Moreover, due to the long wavelength of the cycloid, exchange anisotropy can be effectively absorbed into the single-ion anisotropy (SIA) $K > 0$, which favors spin alignment along $\mathbf{z}'$. All terms in this Hamiltonian are also essential to explain the spin modes of $BiFeO_3$ observed using THz spectroscopy [21, 22].

Since the FE distortion is uniform, the $\boldsymbol{D}_{FE}$ sum is translation invariant. Due to the translation-odd $R_4^+[111]$ AF octahedral rotation, the $\boldsymbol{D}_{AF}$ sum contains the coefficient $(-1)^{n_i}$, which alternates from one hexagonal layer $n_i = \sqrt{3}\,\mathbf{z}' \cdot \mathbf{R}_i/a$ to the next. Simplified forms for the DM terms $\mathcal{H}^{SC}_{FE}$ and $\mathcal{H}^{SC}_{AF}$ are given in appendix A.

By ignoring the higher cycloidal harmonics but including the tilt [23] τ produced by $\boldsymbol{D}_{AF}$, the classiscl spin state can be approximated [24] as

$$S_{x'}(\mathbf{R}) = S(-1)^{n+1}\cos\tau\sin(2\pi\delta r), \tag{7}$$

$$S_{y'}(\mathbf{R}) = S\sin\tau\sin(2\pi\delta r), \tag{8}$$

Table 1. Calculated magnetic interaction parameters (meV) compared to spin model results fitted to neutron-scattering measurements [22]. D_{AF} splits into two components parallel ($A = 0.042$) and perpendicular ($B = 0.075$) to spin bond direction. The components A and B are explained in appendix A.2.

meV	J_1	D_{FE}	D_{AF}	K
LSDA+U	−6.1	0.089	0.042, 0.075	3.5×10^{-3}
Neutron	−5.3	0.103	0.064	4.1×10^{-3}

$$S_{z'}(\mathbf{R}) = S(-1)^{n+1}\cos(2\pi\delta r), \tag{9}$$

so that the spins on each hexagonal layer depend only on the integer $r = \sqrt{2}\,\mathbf{x}' \cdot \mathbf{R}/a$. The weak FM moment $\mathbf{M}_0 = 2\mu_B S_0 \mathbf{y}'$ of the canted antiferromagnetic phase above H_c is related to the tilt by [21] $\sin\tau = S_0/S$. For [5, 25] $M_0 = 0.03\,\mu_B$, $\tau = 0.006$ or $0.34°$. By comparison, the local spin-density approximation (LSDA)+U ($U = 5$ eV) calculations described in the next section yield $M_0 = 0.029\,\mu_B$. Because higher harmonics are neglected, averages taken with the tilted cycloid in zero magnetic field introduce a very small error of order 10^{-5}. Quantum fluctuations about the classical spin state are expected to be small for $S = 5/2$ Fe^{3+} ions.

2. First-principles method

First-principles calculations were performed using density functional theory (DFT) from the VASP code within LSDA+U. The Hubbard $U = 5$ eV and the exchange $J_H = 0$ eV parameters were optimized for Fe^{3+} in $BiFeO_3$ [26, 27]. We employed projector augmented wave potentials [28, 29]. To integrate over the Brillouin zone, we constructed a supercell made of $2 \times 2 \times 2$ perovskite units (40 atoms, 8 f.u.) and a $3 \times 3 \times 3$ Monkhorst–Pack k-points mesh. The DM interactions $\mathbf{D}_{FE}$ and $\mathbf{D}_{AF}$ were evaluated with $4 \times 2 \times 2$ units (80 atoms, 16 f.u.) and a $1 \times 3 \times 3$ Monkhorst–Pack mesh. The wave functions were expanded with plane waves up to an energy cutoff of 500 eV. To calculate exchange interactions (J_n), we applied four different magnetic configurations (G-AFM, C-AFM, A-AFM and FM). We estimated $\mathbf{D}_{FE}$ and $\mathbf{D}_{AF}$ by replacing all except four of the Fe^{3+} cations with Al^{3+} [26] in the 80 atom unit cell. As shown in table 1, the LSDA+U results are in excellent agreement with recent neutron-scattering measurements [22].

After obtaining the exchange, DM, and SIA interactions, we calculate their derivatives with respect to an applied electric field parallel to a cartesian direction. A dielectric constant $\epsilon = 90$ is used to estimate the SD polarizations when the electric field is perpendicular to the rhombohedral axis [30]. To simulate atomic displacements driven by the applied field E_α, we evaluate the lowest-frequency polar eigenvector from the dynamical matrix by forcibly moving the atoms incrementally from the ground state $R3c$ structure. The resulting energy difference between the two structures is divided by the induced electric polarization P_α^{ind}. The major difference in the polar eigenvectors obtained from the dynamic and the force-constant matrices arises from the Fe–O–Fe bond angle. The eigenvectors of the dynamic matrix reduce the bond-angle while the eigenvectors of the force-constant matrix raises that angle (see appendix B). These opposing tendencies produce distinct ME behaviors for dynamic and static electric fields. Although this paper evaluates the SD polarizations for dynamic electric fields, the general formalism is applicable in both the static and dynamic limits.

3. SC polarizations

The cross products $\mathbf{S}_i \times \mathbf{S}_j$ modulate the Fe–O–Fe bond angle and produce the SC polarizations [31]. These SC polarizations are simply obtained from electric-field derivatives of Dzyaloshinskii–Moriya interaction Hamiltonian. In $BiFeO_3$, FE and AF distortions generate SC polarizations $\mathbf{P}_{FE}^{SC}$ and $\mathbf{P}_{AF}^{SC}$ associated with the electric-field derivatives of the DM interactions $\mathbf{D}_{FE}$ and $\mathbf{D}_{AF}$. These are calculated using the procedure described in [20].

The first SC polarization is induced by the response of the FE distortion to an external electric field:

$$P_{FE,\gamma}^{SC} = -\frac{1}{N}\frac{\partial \mathcal{H}_{FE}^{SC}}{\partial E_\gamma} = -\frac{1}{N}\sum_{u,\langle i,j\rangle^{\mathbf{u}}}\frac{\partial \mathbf{D}_{FE}^u}{\partial E_\gamma}\cdot(\mathbf{S}_i \times \mathbf{S}_j), \tag{10}$$

where $\langle i, j\rangle^{\mathbf{u}}$ is a sum over nearest neighbors with $\mathbf{R}_j - \mathbf{R}_i = a\mathbf{u}$ and $\mathbf{u} = \mathbf{x}$, $\mathbf{y}$, or $\mathbf{z}$ cubic axis. The electric-field derivatives of the DM interactions $\mathbf{f}^{u\gamma} = \partial \mathbf{D}_{FE}^u/\partial E_\gamma$ are given in appendix C and table 2. While the derivative $\mathbf{f}^{\alpha\alpha}$ of $\mathbf{D}_{FE}^\alpha$ between spins $\mathbf{S}_j$ and $\mathbf{S}_i$ with $\mathbf{R}_j - \mathbf{R}_i$ parallel to the electric field is parallel to $\mathbf{D}_{FE}^\alpha$, the derivative $\mathbf{f}^{\alpha\beta}$ ($\beta \neq \alpha$) of $\mathbf{D}_{FE}^\alpha$ between spins with $\mathbf{R}_j - \mathbf{R}_j$ perpendicular to the electric field is perpendicular to $\mathbf{D}_{FE}^\alpha$, as shown in figure 1.

Table 2. SD polarizations from ES, SC and SIA. Shown are the calculated (LSDA+U) electric-field derivatives of J_1, D_{FE}, D_{AF}, and K. The upper left and right scripts denote the directions of the spin bond and electric field, respectively. $f_\beta^{\alpha\alpha} = -f_\gamma^{\alpha\alpha}$, $f_\gamma^{\alpha\beta} = -f_\gamma^{\beta\alpha}$, and $a_\beta^{\alpha\alpha} = a_\gamma^{\alpha\alpha}$ by $R3c$ symmetry as in appendix C. α, β, and γ are in ascending order so that $\epsilon_{\alpha\beta\gamma} = 1$. All units are nC cm^{-2}.

| | SC polarization from | | | | | ES polarization | |
| | D_{FE} | | | SC polarization from D_{AF} | | from J_1 | |
	$f_\beta^{\alpha\alpha}$	$f_\gamma^{\alpha\beta}$	$f_\beta^{\alpha\beta}$	$a_\alpha^{\alpha\alpha} + 2a_\beta^{\alpha\beta}$	$a_\beta^{\alpha\alpha} + a_\alpha^{\alpha\beta} + a_\gamma^{\alpha\beta}$	C_{AF}	C_{FE}
LSDA+U	9	17	14	17	-19	-250	-350
NDD	36	29	29	28	-7.2	—	—

Figure 1. Influence of electric fields on the DM interactions. Blue arrows denote DM vectors without **E** and red arrows denote the change of the DM interactions with **E**. (a) FE-induced DM (D_{FE}) and its derivative vectors (**f**) with respect to **E**. (b) AF-induced DM (D_{AF}) and its derivative vectors (**a**) with respect to **E**. The signs of the vectors alternate due to the AF rotations. Thick- and light-red arrows denote responses of DM to **E** along the α direction when bonds between Fe ions are parallel (**f**$^{\alpha\alpha}$, **a**$^{\alpha\alpha}$) and perpendicular (**f**$^{\alpha\beta}$, **a**$^{\alpha\beta}$) to **E**, respectively. The size of the arrows is proportional to the magnitude of the response to **E**. O$^{\alpha\alpha}$ (O$^{\alpha\beta}$) denotes oxygens along bonds parallel (perpendicular) to **E**. Bi atoms are not drawn for clarity.

In the lab reference frame $\{x, y, z\}$, regrouping terms for domain 2 with $\mathbf{x}' = [1, 0, -1]$ using equations (7)–(9) yields

$$\mathbf{P}_{FE}^{SC} = -\frac{1}{N} \underline{\Delta}^{FE} \cdot \sum_{\langle i,j \rangle^{\mathbf{x}}} (\mathbf{S}_i \times \mathbf{S}_j), \qquad (11)$$

where

$$\underline{\Delta}^{FE} = \begin{pmatrix} \mathbf{f}^{xx} \\ \mathbf{f}^{xy} \\ \mathbf{f}^{xz} \end{pmatrix} - \begin{pmatrix} \mathbf{f}^{zx} \\ \mathbf{f}^{zy} \\ \mathbf{f}^{zz} \end{pmatrix} = \begin{pmatrix} -h & f-g & -f \\ g & 2h & g \\ -f & f-g & -h \end{pmatrix} \qquad (12)$$

with $f = f_\beta^{\alpha\alpha}$, $g = f_\beta^{\alpha\beta}$, and $h = f_\gamma^{\alpha\beta}$ given in table 2. Fits to the NDD [19] described in section 6 imply that $g = h$.

The second SC polarization alternates in sign due to the alternating AF rotations along [111]:

$$P_{AF,\gamma}^{SC} = -\frac{1}{N} \frac{\partial \mathcal{H}_{AF}^{SC}}{\partial E_\gamma} = -\frac{1}{N} \sum_{u, \langle i,j \rangle^{\mathbf{u}}} (-1)^{n_i} \frac{D_{AF}^u}{\partial E_\gamma} \cdot (\mathbf{S}_i \times \mathbf{S}_j). \qquad (13)$$

The SC polarization components $a^{u\gamma} = \partial D_{AF}^u / \partial E_\gamma$ are evaluated in table 2. While the derivative $\mathbf{a}^{\alpha\alpha}$ of D_{AF}^α between spins $\mathbf{S}_i$ and $\mathbf{S}_j$ with $\mathbf{R}_j - \mathbf{R}_i$ parallel to the electric field is nearly anti-parallel to D_{AF}^α, the derivative $\mathbf{a}^{\alpha\beta}$ ($\beta \neq \alpha$) of D_{AF}^α between spins with $\mathbf{R}_j - \mathbf{R}_i$ perpendicular to the electric field is perpendicular to D_{AF}^α, as shown in figure 1.

Appendix D shows that the SC polarization can be simplified as

$$\mathbf{P}_{AF}^{SC} = \frac{1}{\sqrt{3}N} \underline{\Delta}^{AF} \cdot \sum_{u, \langle i,j \rangle^{\mathbf{u}}} (-1)^{n_i} (\mathbf{S}_i \times \mathbf{S}_j), \qquad (14)$$

where

$$\underline{\Lambda}^{\mathrm{AF}} = \mathbf{a}^{xx} + \mathbf{a}^{yy} + \mathbf{a}^{zz} = \begin{pmatrix} s & t & t \\ t & s & t \\ t & t & s \end{pmatrix} \qquad (15)$$

with $s = a_\alpha^{\alpha\alpha} + 2a_\beta^{\alpha\beta}$ and $t = a_\beta^{\alpha\alpha} + a_\alpha^{\alpha\beta} + a_\gamma^{\alpha\beta}$ given in table 2.

4. ES polarizations

The absence of an inversion center between neighboring spin sites induces the ES bond polarizations. Since the scalar product $\mathbf{S}_i \cdot \mathbf{S}_j$ is altered by external perturbations such as temperature, electric field, or magnetic field, FE and AF distortions each generates its own ES polarization.

For symmetric exchange couplings, ES is dominated by the response of the nearest-neighbor interaction J_1:

$$\mathcal{H}_{\mathrm{ex}} = -\sum_{\langle i,j \rangle} J_1 \, \mathbf{S}_i \cdot \mathbf{S}_j = -\sum_{u,\langle i,j \rangle^{\mathbf{u}}} J_1^u \, \mathbf{S}_i \cdot \mathbf{S}_j. \qquad (16)$$

The two ES polarizations $\mathbf{P}_{\mathrm{FE}}^{\mathrm{ES}}$ and $\mathbf{P}_{\mathrm{AF}}^{\mathrm{ES}}$ are closely related to one another. The electric-field derivatives $\underline{\Gamma}$ are given in the cubic coordinate system by

$$P_{\mathrm{FE},\alpha}^{\mathrm{ES}} = -\frac{1}{N} \frac{\partial \mathcal{H}_{\mathrm{ex}}}{\partial E_\alpha} = \sum_\beta \Gamma_{\alpha\beta}^{\mathrm{FE}} \, W_{1\beta}, \qquad (17)$$

$$\underline{\Gamma}^{\mathrm{FE}} = \begin{pmatrix} C_\parallel & C_\perp & C_\perp \\ C_\perp & C_\parallel & C_\perp \\ C_\perp & C_\perp & C_\parallel \end{pmatrix}, \qquad (18)$$

$$W_{1u} = \frac{1}{N} \sum_{\langle i,j \rangle^{\mathbf{u}}} \mathbf{S}_i \cdot \mathbf{S}_j, \qquad (19)$$

where $C_\perp = \partial J_1^\beta / \partial E_\alpha \ (\beta \neq \alpha)$ and $C_\parallel = \partial J_1^\alpha / \partial E_\alpha$ for spin bonds perpendicular and parallel to the electric field, respectively.

Because the AF octahedral rotation is perpendicular to $\mathbf{z}'$, the ES polarization associated with AF rotations is also perpendicular to $\mathbf{z}'$ with

$$\boldsymbol{P}_{\mathrm{AF}}^{\mathrm{ES}} = C_{\mathrm{AF}} \, \mathbf{z}' \times \mathbf{W}_2, \qquad (20)$$

$$P_{\mathrm{AF},\alpha}^{\mathrm{ES}} = \sum_\beta \Gamma_{\alpha\beta}^{\mathrm{AF}} \, W_{2\beta}, \qquad (21)$$

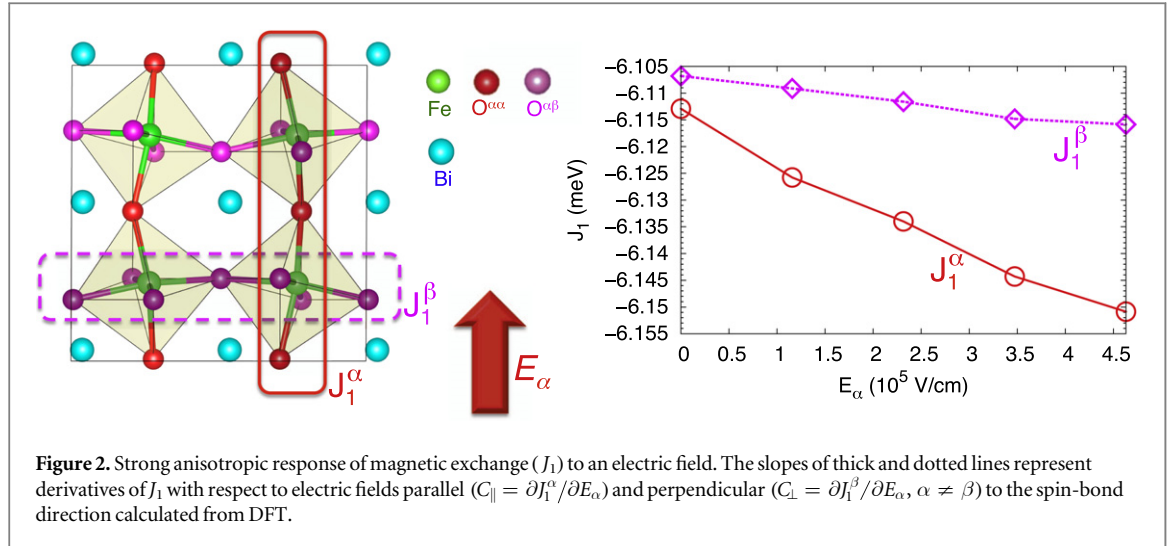$$W_{2u} = \frac{1}{N} \sum_{\langle i,j \rangle^{\mathbf{u}}} (-1)^{n_i} \, \mathbf{S}_i \cdot \mathbf{S}_j, \qquad (22)$$

$$\underline{\Gamma}^{\mathrm{AF}} = \begin{pmatrix} 0 & -(C_\parallel - C_\perp) & C_\parallel - C_\perp \\ C_\parallel - C_\perp & 0 & -(C_\parallel - C_\perp) \\ -(C_\parallel - C_\perp) & C_\parallel - C_\perp & 0 \end{pmatrix}. \qquad (23)$$

Unlike W_{1u}, W_{2u} alternates in sign due to the opposite AF rotations on adjacent hexagonal layers.

The first ES polarization parallel to $\mathbf{z}'$ with coefficient $C_{\mathrm{FE}} = 2C_\perp + C_\parallel$ modulates the FE polarization that already breaks IS above T_{N}. The second ES polarization perpendicular to $\mathbf{z}'$ has coefficient $C_{\mathrm{AF}} = C_\perp - C_\parallel$. The AF rotations affect the bonds between nearest-neighbor spins in the plane normal to $\mathbf{z}'$ because each oxygen moves along the directions $[0, -1, 1]$, $[1, 0, -1]$, and $[-1, 1, 0]$, perpendicular to $\mathbf{z}'$. Thus, the second ES polarization is associated with atomic displacements perpendicular to $\mathbf{z}'$ and parallel to the AF rotation.

Figure 2 demonstrates the strong anisotropy in the response of magnetic exchange to an electric field. While $C_\perp$ arises from the change in Fe–O–Fe bond angle due to a polar distortion, $C_\parallel$ arises from bond contraction. As shown, $C_\parallel$ is much more sensitive to an electric field than $C_\perp$. Since the ME anisotropy $C_{\mathrm{AF}} = C_\parallel - C_\perp$ produces an ES polarization, the AF rotation angle is changed by the spin ordering. In particular, the negative sign of $C_{\mathrm{AF}} = -250 \ \mathrm{nC \ cm}^{-2}$ indicates that the rotation angle increases with the dot product $\mathbf{S}_i \cdot \mathbf{S}_j$ because oxygen atoms moving in the AF plane have a negative effective charge $Z_{\mathrm{O}}^*(\mathrm{DFT}) = -3.3e$.

The anisotropic ES polarization components $C_\perp$ and $C_\parallel$ cooperatively induce the ES polarization along $\mathbf{z}'$ under the IS broken by the FE polarization. In contrast to our previous study [20] on the response to a *static* electric field ($C_{\mathrm{FE}} = 215 \ \mathrm{nC \ cm}^{-2}$), we obtain a negative $C_{\mathrm{FE}} = -350 \ \mathrm{nC \ cm}^{-2}$ in a dynamic electric field. Appendix B describes the different eigenvectors of the dynamic and force-constant matrices. While Fe moves upward with respect to oxygen in the static regime, Fe moves downward in the dynamic regime because its mass

Figure 2. Strong anisotropic response of magnetic exchange (J_1) to an electric field. The slopes of thick and dotted lines represent derivatives of J_1 with respect to electric fields parallel ($C_\parallel = \partial J_1^\alpha / \partial E_\alpha$) and perpendicular ($C_\perp = \partial J_1^\beta / \partial E_\alpha$, $\alpha \neq \beta$) to the spin-bond direction calculated from DFT.

is much larger than that of oxygen. Therefore, a static **E** increases the bond angle of Fe–O–Fe (positive C_{FE}) but a dynamic **E** decreases the bond angle (negative C_{FE}) due to the Goodenough–Kanamori rules [32].

We recently predicted [20] that the *static* SD polarization of BiFeO$_3$ is about $-3\,\mu$C cm^{-2} along a cubic diagonal opposite to the FE polarization emerging below T_C. The electronic plus atomic contribution to the SD polarization is $-1.3\,\mu$C cm^{-2} and the lattice-deformation contribution is $-1.7\,\mu$C cm^{-2}, which were slightly underestimated (-1.0 and -1.3, respectively) in previous literature [33, 34]. The total SD polarization ($-3\,\mu$C cm^{-2}) is higher than observed in any other known multiferroic material [20].

5. Origin of NDD

The most stringent test yet for the microscopic model proposed above is its ability to predict the NDD which is the asymmetry $\Delta\alpha(\omega)$ in the absorption $\alpha(\omega)$ of light when the direction of light propagation is reversed. The absorption of THz light is given by $\alpha(\omega) = (2\omega/c)\mathrm{Im}N(\omega)_{ij}$, where [35, 36]

$$N(\omega)_{ij} \approx \sqrt{(\epsilon_{ii} + \chi_{ii}^{ee}(\omega))(1 + \chi_{jj}^{mm}(\omega))} \pm \chi_{ji}^{me}(\omega) \qquad (24)$$

is the complex refractive index for a linearly polarized beam, $\underline{\chi}^{ee}$, $\underline{\chi}^{mm}$ and $\underline{\chi}^{me}$ are the dielectric, magnetic, and magnetoelectric susceptibility tensors describing the dynamical response of the spin system [13, 15, 17, 35] and $\underline{\epsilon}$ is the dielectric constant related to the charge response. Subscripts i and j are fixed by the electric **e** and magnetic **h** polarization directions, respectively. The second term, which depends on the light propagation direction and produces NDD, is separated from the mean absorption by writing $N(\omega)_{ij} = \bar{N}(\omega) \pm \chi_{ji}^{me}(\omega)$.

Summing over the spin-wave modes n at the cycloidal ordering wavevector **Q**, $\Delta\alpha(\omega) = (4\omega/c)\mathrm{Im}\chi_{ji}^{me}(\omega)$ is given by

$$\Delta\alpha(\omega) = \sum_n A_n\,\delta(\omega - \omega_n), \qquad (25)$$

$$A_n = NX\omega_n\,\mathrm{Re}\,\{\rho_{n0}\mu_{0n}\}, \qquad (26)$$

$$\rho_{0n} = \langle 0|\mathbf{P}^{SD}\cdot\mathbf{e}/\mathcal{V}|n\rangle, \qquad \mu_{0n} = \langle 0|\mathbf{M}\cdot\mathbf{h}/\mu_B|n\rangle, \qquad (27)$$

where $\mathbf{M} = (2\mu_B/N)\sum_i \mathbf{S}_i$ is the magnetization, $\mathcal{V} = a^3$ is the volume per Fe site, $\mathbf{P}^{SD}/\mathcal{V} = (\mathbf{P}^{ES} + \mathbf{P}^{SC})/\mathcal{V}$ is the net SD polarization given in units of, nC cm^{-2}, and $X = (4\pi\mu_B/\hbar)$ nC cm$^{-2} = 0.1388$ cm^{-1}.

For each field orientation, the integrated weight of every spectroscopic peak at ω_n is compared with the measured values, thereby eliminating estimates of the individual peak widths. Experimental results for the NDD with field along $\mathbf{m} = [1, -1, 0]$ are plotted in figure 3(a) for $\mathbf{e} = [1, -1, 0]$. Fits to the NDD are based on the plotted 2, 4, 6, 8, 10, and 12 T data sets. For each data set, we evaluate the integrated weights for the eight modes [22] Ψ_0, $\Phi_1^{(1)}$, $\Psi_1^{(1,2)}$, $\Phi_2^{(1,2)}$, and $\Psi_2^{(1,2)}$ between roughly 12 and 35 cm^{-1}.

Comparing figures 3(a) and (b), the NDD for $\mathbf{m} = [1, -1, 0]$ is dominated by the two sets of SC polarizations $\mathbf{P}_{FE}^{SC}$ and $\mathbf{P}_{AF}^{SC}$. Table 2 indicates that the fitting results are not significantly changed by including the ES polarizations. Figure 3(c) attempts to fit the experimental data using the ES polarizations alone. Clearly, the ES polarizations by themselves cannot produce the observed NDD.

Figures 3(a) and (b) indicate that the various components of the SC polarizations in BiFeO$_3$ are captured by first-principles calculations and that the NDD is not strongly affected by the ES terms This selectivity originates
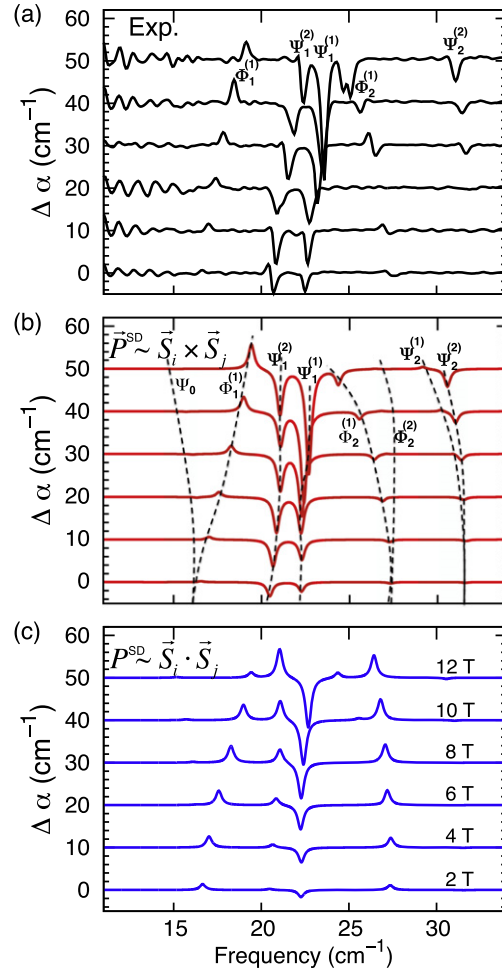
Figure 3. Origin of the strong NDD in BiFeO$_3$. (a) The experimental NDD ($\Delta\alpha$) with static magnetic field from 2 to 12 T and oscillating electric field along $[1, -1, 0]$. The predicted NDD using (b) SC and (c) ES polarizations. Here, i, j denote nearest neighbors.
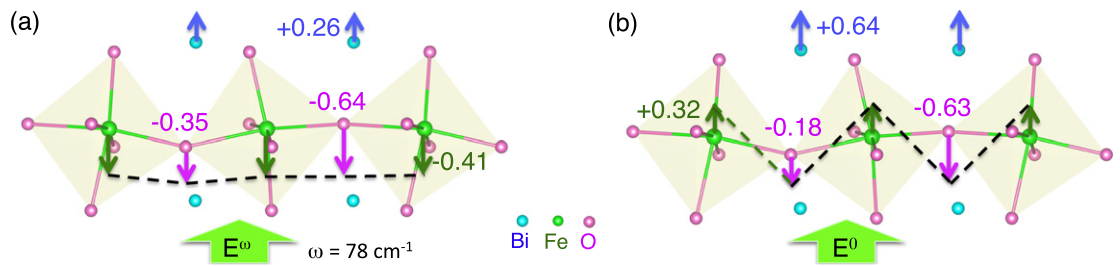

Figure 4. Distinct atomic responses to dynamic and static electric fields. The lowest-frequency eigenvectors of (a) dynamic and (b) force-constant matrices are compared. Note that the polar displacement in the dynamic limit ($\omega = 78$ cm^{-1}) increases the Fe–O–Fe bond angle (dotted line) while the displacement decreases the bond angle in the static limit.

from the spin dynamics of this nearly collinear antiferromagnet. Due to the very small SIA on the $S = 5/2$ Fe^{3+} spins, each magnon mode can be described as the pure precession of Fe^{3+} spins: the oscillating component $\delta\mathbf{S}_i^\omega$ of the spin on site i is perpendicular to its equilibrium direction $\mathbf{S}_i^0$. Since neighboring spins in the long-wavelength spin cycloid of BiFeO$_3$ are close to collinear, a dynamic polarization is effectively induced by SC terms such as $\mathbf{S}_i^0 \times \delta\mathbf{S}_{i+1}^\omega$. However, the dynamic polarization generated by ES terms $\mathbf{S}_i^0 \cdot \delta\mathbf{S}_{i+1}^\omega$ is almost zero. The spin stretching modes observed in strongly anisotropic magnets [35, 38] do not appear in BiFeO$_3$.

Recent work [37] explains the observed *static* polarization perpendicular to $\mathbf{z}'$ by the $\mathbf{z}' \times \mathbf{P}_{FE}^{SC}$ term proportional to $h - f$. Although the fitting and LSDA+U values for $h - f \equiv f_\gamma^{\alpha\beta} - f_\beta^{\alpha\alpha} \sim \pm 10$ nC cm^{-2} in

table 2 are an order of magnitude smaller than required by that work, keep in mind that the SC parameters given in table 2 were evaluated or fitted for a dynamic electric field.

Although DFT calculations underestimate the ME coefficients compared to the NDD fitting results in table 2, they nicely demonstrate which of the symmetry-allowed ME couplings are relevant and which are negligibly small. Combining the two methodologies allows a more unambiguous determination of these coupling parameters. There are several possible explanations for the difference between the results obtained from DFT calculations and the NDD fitting. First, a larger dielectric constant ϵ could produce better agreement between DFT and NDD since the SD polarizations are proportional to ϵ through

$$P_\alpha^{SD} = \frac{\partial \mathcal{H}}{\partial E_\alpha} = \frac{\partial P_\alpha^{ind}}{\partial E_\alpha} \frac{\partial \mathcal{H}}{\partial P_\alpha^{ind}} \approx \epsilon \frac{\partial \mathcal{H}}{\partial P_\alpha^{ind}}. \tag{28}$$

Second, higher-frequency polar modes not considered here also can affect NDD. Third, a smaller Hubbard U will increase the SD polarizations and improve the agreement with the experimental fits. Fourth, magnon modes were observed between $\nu = 15$ and $40 \ \mathrm{cm}^{-1}$ while we calculated the SC coupling constants in the dynamical limit. The crossover frequency ω_c between static and dynamical behavior lies between 0 and the polar phonon at $\omega = 78 \ \mathrm{cm}^{-1}$. If ω_c lies in the middle of the measured frequencies, then the SC fitting parameters may differ from the dynamical couplings obtained from LSDA $+U$.

6. Discussion

In order to study the ME couplings in complex multiferroic systems, first-principles calculations must be anchored to the right microscopic Hamiltonian. With two sets of SC polarizations derived from the two distinct structural distortions, BiFeO$_3$ is a good example of how our atomistic approach works for complex materials. This paper calculated only the ionic displacement contribution to the ME coupling which is typically larger than the purely electronic contribution [34, 39]. The lattice deformation contribution to the SD polarization was discussed in our previous work [20].

The higher-frequency polar modes contribute to the electric-field induced displacement. Their contributions are proportional to the mode strength Z^2/ω^2, where Z is the mode effective charge and ω its frequency. From our dynamical matrix calculations, the mode strengths of the higher frequency modes are less than 30% smaller than the strength of the lowest mode. Therefore, the lowest mode makes dominates the electric-field induced polar displacement.

The advantages (large FE polarization, high T_C, and high T_N) of BiFeO$_3$ are also major obstacles to understanding the ME couplings that produce the SD polarizations below T_N. Leakage currents and the preexisting large FE polarization at high temperatures have hampered magneto-capacitance measurements and hidden the SD polarizations. Although recent neutron-scattering measurements [10] imply a large ES polarization, most other ME polarizations are unknown. We show that NDD measurements combined with first-principles calculations based on a microscopic model reveal the hidden SC polarizations. In particular, this approach allows us to disentangle the delicate SC polarizations and the hidden ES polarizations associated with AF rotations. We envision that intrinsic methods such as NDD will reveal hidden ME couplings in many materials and rekindle the investigation of type-*I* multiferroics.

Acknowledgments

Appendix A. Simplified form for the Dzyaloshinskii–Moriya interactions

A.1. FE-induced Dzyaloshinskii–Moriya interaction
Since the FE vectors $\boldsymbol{D}_{FE}^u$ are given by $(0, D_{FE}, -D_{FE})$, $(-D_{FE}, D_{FE}, 0)$, and $(D_{FE}, -D_{FE}, 0)$ between nearest spins along $\mathbf{x}$, $\mathbf{y}$, and $\mathbf{z}$, respectively, the FE-induced DM interaction can be transformed as:

$$\mathcal{H}_{\mathrm{FE}}^{\mathrm{SC}} = \sum_{\mathbf{R}_i, \mathbf{R}_j = \mathbf{R}_i + a\mathbf{u}} \boldsymbol{D}_{\mathrm{FE}}^{u} \cdot (\mathbf{S}_i \times \mathbf{S}_j)$$

$$= D_1 \sum_{\mathbf{R}_i, \mathbf{R}_j = \mathbf{R}_i + a\mathbf{u}} (\mathbf{z}' \times \mathbf{u}) \cdot (\mathbf{S}_i \times \mathbf{S}_j), \tag{A1}$$

where $D_1 = D_{\mathrm{FE}} \approx 0.154$ meV is now larger by $\sqrt{2}$ than in previous work [21].

A.2. AF-induced Dzyaloshinskii–Moriya interaction

The AF interactions $\boldsymbol{D}_{\mathrm{AF}}^{u}$ along $\mathbf{x}$, $\mathbf{y}$, and $\mathbf{z}$ can be written

$$\boldsymbol{D}_{\mathrm{AF}}^{x} = B(\mathbf{y} + \mathbf{z}) + A\mathbf{x}, \tag{A2}$$

$$\boldsymbol{D}_{\mathrm{AF}}^{y} = B(\mathbf{z} + \mathbf{x}) + A\mathbf{y}, \tag{A3}$$

$$\boldsymbol{D}_{\mathrm{AF}}^{z} = B(\mathbf{x} + \mathbf{y}) + A\mathbf{z}. \tag{A4}$$

For domain 2 with $\mathbf{x}' = [1, 0, -1]$,

$$\begin{aligned}
\mathcal{H}_{\mathrm{AF}}^{\mathrm{SC}} &= \sum_{\mathbf{R}_i, \mathbf{R}_j = \mathbf{R}_i + a\mathbf{u}} (-1)^{n_i} \boldsymbol{D}_{\mathrm{AF}}^{u} \cdot (\mathbf{S}_i \times \mathbf{S}_j) \\
&= \sqrt{3} \sum_{\mathbf{R}_i}' \mathbf{z}' \cdot \{ B\, \mathbf{S}_r \times (\mathbf{S}_{\mathbf{R}_i + a\mathbf{x}} + 2\mathbf{S}_{\mathbf{R}_i + a\mathbf{y}} + \mathbf{S}_{\mathbf{R}_i + a\mathbf{z}}) \\
&\qquad + A\, \mathbf{S}_{\mathbf{R}_i} \times (\mathbf{S}_{\mathbf{R}_i + a\mathbf{x}} + \mathbf{S}_{\mathbf{R}_i + a\mathbf{z}}) \} \\
&\quad + \sum_{\mathbf{R}_i}' \mathbf{y}' \cdot \{ (B - A)\, \mathbf{S}_{\mathbf{R}_i} \times (\mathbf{S}_{\mathbf{R}_i + a\mathbf{x}} - 2\mathbf{S}_{\mathbf{R}_i + a\mathbf{y}} + \mathbf{S}_{\mathbf{R}_i + a\mathbf{z}}) \} \\
&\approx \sqrt{3} \sum_{\mathbf{R}_i}' \mathbf{z}' \cdot \{ B\, \mathbf{S}_{\mathbf{R}_i} \times (\mathbf{S}_{\mathbf{R}_i + a\mathbf{x}} + 2\mathbf{S}_{\mathbf{R}_i + a\mathbf{y}} + \mathbf{S}_{\mathbf{R}_i + a\mathbf{z}}) \\
&\qquad + A\, \mathbf{S}_{\mathbf{R}_i} \times (\mathbf{S}_{\mathbf{R}_i + a\mathbf{x}} + \mathbf{S}_{\mathbf{R}_i + a\mathbf{z}}) \}, \\
&\approx \sqrt{3}\,(4B + 2A) \sum_{\mathbf{R}_i}' \mathbf{z}' \cdot (\mathbf{S}_{\mathbf{R}_i} \times \mathbf{S}_{\mathbf{R}_i + a\mathbf{y}}),
\end{aligned} \tag{A5}$$

where the primed sum over $\mathbf{R}_i$ is restricted to either n_i odd or even hexagonal layers. Based on the tilted cycloid of equations (7)–(9) the $\mathbf{z}'$ term dominates because $\mathbf{S}_{\mathbf{R}_i + a\mathbf{x}} - 2\mathbf{S}_{\mathbf{R}_i + a\mathbf{y}} + \mathbf{S}_{\mathbf{R}_i + a\mathbf{z}}$ is of order $\delta^2 \sim 2 \times 10^{-5}$.

Previously, the second DM term was written

$$\begin{aligned}
\mathcal{H}_{\mathrm{AF}}^{\mathrm{SC}} &= D_2 \sum_{\mathbf{R}_i, \mathbf{R}_j = \mathbf{R}_i + a\mathbf{u}} (-1)^{n_i} \mathbf{z}' \cdot (\mathbf{S}_i \times \mathbf{S}_j) \\
&= 2\sqrt{3} D_2 \sum_{\mathbf{R}_i}' \mathbf{z}' \cdot (\mathbf{S}_{\mathbf{R}_i} \times \mathbf{S}_{\mathbf{R}_i + a\mathbf{x}} + \mathbf{S}_{\mathbf{R}_i} \times \mathbf{S}_{\mathbf{R}_i + a\mathbf{y}} + \mathbf{S}_{\mathbf{R}_i} \times \mathbf{S}_{\mathbf{R}_i + a\mathbf{z}}) \\
&\approx 6\sqrt{3} D_2 \sum_{\mathbf{R}_i}' \mathbf{z}' \cdot (\mathbf{S}_{\mathbf{R}_i} \times \mathbf{S}_{\mathbf{R}_i + a\mathbf{y}}),
\end{aligned} \tag{A6}$$

which also uses equations (7)–(9). Therefore, $D_2 = (A + 2B)/3 = 0.064$ meV, which is in excellent agreement with previous work [21].

Appendix B. Eigenvectors of dynamic and force-constant matrices

As noted in section 4, C_{FE} is negative from the eigenmode of the dynamic matrix while it is positive from the eigenmode of the force-constant matrix [20]. This difference originates from the opposite changes to the Fe–O–Fe bond angle: the bond angle increases in the static limit while it decreases in the dynamic limit.

Appendix C. Spin-current polarization components

Defining $\mathbf{f}^{u\gamma} = \partial \boldsymbol{D}_{\mathrm{FE}}^{u} / \partial E_\gamma$,

$$\boldsymbol{D}_{\mathrm{FE}}^{x} = (0, D, -D), \qquad \boldsymbol{D}_{\mathrm{FE}}^{y} = (-D, 0, D), \qquad \boldsymbol{D}_{\mathrm{FE}}^{z} = (D, -D, 0) \tag{C1}$$

$$\mathbf{f}^{xx} = (0, f, -f), \qquad \mathbf{f}^{yx} = (-g, 0, -h), \qquad \mathbf{f}^{zx} = (g, h, 0), \tag{C2}$$

$$\mathbf{f}^{xy} = (0, g, h), \qquad \mathbf{f}^{yy} = (-f, 0, f), \qquad \mathbf{f}^{zy} = (-h, -g, 0), \tag{C3}$$

$$\mathbf{f}^{xz} = (0, -h, -g), \qquad \mathbf{f}^{yz} = (h, 0, g), \qquad \mathbf{f}^{zz} = (f, -f, 0), \tag{C4}$$

where $f \equiv f_\beta^{\alpha\alpha}$, $g \equiv f_\beta^{\alpha\beta}$, and $h \equiv f_\gamma^{\alpha\beta}$.

Defining $\mathbf{a}^{u\gamma} = \partial \boldsymbol{D}_{\mathrm{AF}}^u / \partial E_\gamma$,

$$\boldsymbol{D}_{\mathrm{FE}}^x = (A, B, B), \qquad \boldsymbol{D}_{\mathrm{FE}}^y = (B, A, B), \qquad \boldsymbol{D}_{\mathrm{FE}}^z = (B, B, A), \tag{C5}$$

$$\mathbf{a}^{xx} = (a, b, b), \qquad \mathbf{a}^{yx} = (d, c, e), \qquad \mathbf{a}^{zx} = (d, e, c), \tag{C6}$$

$$\mathbf{a}^{xy} = (c, d, e), \qquad \mathbf{a}^{yy} = (b, a, b), \qquad \mathbf{a}^{zy} = (e, d, c), \tag{C7}$$

$$\mathbf{a}^{xz} = (c, e, d), \qquad \mathbf{a}^{yz} = (e, c, d), \qquad \mathbf{a}^{zz} = (b, b, a), \tag{C8}$$

where $a \equiv a_\alpha^{\alpha\alpha}$, $b \equiv a_\beta^{\alpha\alpha}$, $c \equiv a_\alpha^{\alpha\beta}$, $d \equiv a_\beta^{\alpha\beta}$, and $e \equiv a_\gamma^{\alpha\beta}$.

Appendix D. SC polarization from antiferrodistortive Dzyaloshinskii–Moriya coupling

For domain 2 with $\mathbf{x}' = [1, 0, -1]$

$$\mathcal{T}_x = \frac{1}{\sqrt{3}} \mathcal{T}_{z'} - \frac{1}{\sqrt{6}} \mathcal{T}_{y'} \quad \mathcal{T}_y = \frac{\sqrt{6}}{3} \mathcal{T}_{y'} + \frac{1}{\sqrt{3}} \mathcal{T}_{z'} \quad \mathcal{T}_z = \mathcal{T}_x, \tag{D1}$$

which use

$$\mathcal{T}_u \equiv \frac{3}{N} \sum_i (-1)^{n_i} (\mathbf{S}_i \times \mathbf{S}_{i+u}). \tag{D2}$$

The SD polarization associated with $\boldsymbol{D}_{\mathrm{AF}}$ is

$$P_x^{\mathrm{SC}} = \mathbf{a}^{xx} \cdot \mathcal{T}_x + \mathbf{a}^{yx} \cdot \mathcal{T}_y + \mathbf{a}^{zx} \cdot \mathcal{T}_z \tag{D3}$$

$$= \frac{1}{\sqrt{6}} (-\mathbf{a}^{xx} + 2\mathbf{a}^{yx} - \mathbf{a}^{zx}) \cdot \mathcal{T}_{y'} + \frac{1}{\sqrt{3}} (\mathbf{a}^{xx} + \mathbf{a}^{yy} + \mathbf{a}^{zz}) \cdot \mathcal{T}_{z'} \tag{D4}$$

$$\approx \frac{1}{\sqrt{3}} (\mathbf{a}^{xx} + \mathbf{a}^{yy} + \mathbf{a}^{zz}) \cdot \mathcal{T}_{z'}. \tag{D5}$$

Similarly

$$P_y^{\mathrm{SC}} \approx \frac{1}{\sqrt{3}} (\mathbf{a}^{xx} + \mathbf{a}^{yy} + \mathbf{a}^{zz}) \cdot \mathcal{T}_{z'}, \tag{D6}$$

$$P_z^{\mathrm{SC}} \approx \frac{1}{\sqrt{3}} (\mathbf{a}^{xx} + \mathbf{a}^{yy} + \mathbf{a}^{zz}) \cdot \mathcal{T}_{z'}. \tag{D7}$$

So in the local frame

$$P_{\mathbf{x}'}^{\mathrm{SC}} = P_{\mathbf{y}'}^{\mathrm{SC}} = 0, \tag{D8}$$

$$P_{\mathbf{z}'}^{\mathrm{SC}} = \frac{1}{\sqrt{3}} (P_x^{\mathrm{SC}} + P_y^{\mathrm{SC}} + P_z^{\mathrm{SC}}) = \frac{1}{3} (\mathbf{a}^{xx} + \mathbf{a}^{yy} + \mathbf{a}^{zz}) \cdot \mathcal{T}_{z'} \tag{D9}$$

plus a correction of order $\delta^2 \sim 2 \times 10^{-5}$.

The polarization matrix used to evaluate the NDD is given by

$$\mathbf{a}^{xx} + \mathbf{a}^{yy} + \mathbf{a}^{zz} = \begin{pmatrix} a + 2d & b + c + e & b + c + e \\ b + c + e & a + 2d & b + c + e \\ b + c + e & b + c + e & a + 2d \end{pmatrix}, \tag{D10}$$

where $a + 2d = 17 \; \mathrm{nC \, cm}^{-2}$ and $b + c + e = -19 \; \mathrm{nC \, cm}^{-2}$ are obtained from first principles as given in table 2. ($a \equiv a_\alpha^{\alpha\alpha} = 4.1 \; \mathrm{nC \, cm}^{-2}$, $b \equiv a_\beta^{\alpha\alpha} = -21 \; \mathrm{nC \, cm}^{-2}$, $c \equiv a_\alpha^{\alpha\beta} = -6.7 \; \mathrm{nC \, cm}^{-2}$, $d \equiv a_\beta^{\alpha\beta} = 6.4 \; \mathrm{nC \, cm}^{-2}$, and $e \equiv a_\beta^{\alpha\beta} = 8.9 \; \mathrm{nC \, cm}^{-2}$).

References

[1] Teague J R, Gerson R and James W J 1970 *Solid State Commun.* **8** 1073
[2] Sosnowska I, Peterlin-Neumaier T and Steichele E 1982 *J. Phys. C: Solid State Phys.* **15** 4835
[3] Lebeugle D, Colson D, Forget A and Viret M 2007 *Appl. Phys. Lett.* **91** 022907
[4] Kadomtseva A M, Zvezdin A K, Popov Y F, Pyatakov A P and Vorob'ev G P 2004 *JETP Lett.* **79** 571
[5] Tokunaga M, Azuma M and Shimakawa Y 2010 *J. Phys. Soc. Japan* **79** 064713
[6] Park J *et al* 2011 *J. Phys. Soc. Japan* **80** 114714
[7] Lebeugle D, Colson D, Forget A, Viret M, Bataille A M and Gukasov A 2008 *Phys. Rev. Lett.* **100** 227602
[8] Ramazanoglu M, Ratcliff W II, Choi Y J, Lee S, Cheong S-W and Kiryukhin V 2011 *Phys. Rev. B* **83** 174434

[9] Sosnowska I and Przenioslo R 2011 *Phys. Rev. B* **84** 144404

[10] Lee S *et al* 2013 *Phys. Rev. B* **88** 060103(R)

[11] Rovillain P *et al* 2010 *Nat. Mater.* **9** 975

[12] Fiebig M 2005 *J. Phys. D: Appl. Phys.* **38** R123R152

[13] Kézsmárki I, Kida N, Murakawa H, Bordács S, Onose Y and Tokura Y 2011 *Phys. Rev. Lett.* **106** 057403

[14] Takahashi Y, Shimano R, Kaneko Y, Murakawa H and Tokura Y 2012 *Nat. Phys.* **8** 121

[15] Bordács S *et al* 2012 *Nat. Phys.* **8** 734

     Arima T 2008 *J. Phys. Condens. Matter.* **20** 434211

[16] Miyahara S and Furukawa N 2012 *J. Phys. Soc. Japan* **81** 023712

[17] Szaller D, Bordàcs S and Kézsmáki I 2013 *Phys. Rev. B* **87** 014421

     Kézsmáki I *et al* 2014 *Nat. Commun.* **5** 3203

[18] Kézsmáki I *et al* 2015 *Phys. Rev. Lett.* **115** 127203

[19] Fishman R S *et al* 2015 *Phys. Rev. B* **92** 094422

[20] Lee J H and Fishman R S 2015 *Phys. Rev. Lett.* **115** 207203

[21] Fishman R S, Haraldsen J T, Furukawa N and Miyahara S 2013 *Phys. Rev. B* **87** 134416

[22] Nagel U *et al* 2013 *Phys. Rev. Lett.* **110** 257201

[23] Pyatakov A P and Zvezdin A K 2009 *Eur. Phys. J. B* **71** 419

[24] Fishman R S 2013 *Phys. Rev. B* **87** 224419

[25] Zvezdin A K and Pyatakov A P 2012 *Europhys. Lett.* **99** 57003

[26] Weingart C, Spaldin N and Bousquet E 2012 *Phys. Rev. B* **86** 094413

[27] Ederer C and Spaldin N A 2005 *Phys. Rev. B* **71** 060401(R)

[28] Blöchl P E 1994 *Phys. Rev. B* **50** 17953

[29] Kresse G and Joubert D 1999 *Phys. Rev. B* **59** 1758

[30] Lobo R P *et al* 2007 *Phys. Rev. B* **76** 172105

[31] Katsura H, Nagaosa N and Balatsky A V 2005 *Phys. Rev. Lett.* **95** 057205

     Mostovoy M 2006 *Phys. Rev. Lett.* **96** 067601

     Sergienko I A and Dagotto E 2006 *Phys. Rev. B* **73** 094434

[32] Goodenough J B 1993 *Magnetism and the Chemical Bond* (New York: Wiley)

[33] Xiang H J, Wang P S, Whangbo M-H and Gong X G 2013 *Phys. Rev. B* **88** 054404

[34] Lu X Z, Wu X and Xiang H J 2015 *Phys. Rev. B* **91** 100405(R)

[35] Miyahara S and Furukawa N 2011 *J. Phys. Soc. Japan* **80** 073708

[36] Miyahara S and Furukawa N 2014 *Phys. Rev. B* **89** 195145

[37] Tokunaga M *et al* 2015 *Nat. Commun.* **8** 5878

[38] Penc K *et al* 2012 *Phys. Rev. Lett.* **108** 257203

[39] Íñiguez J 2008 *Phys. Rev. Lett.* **101** 117201